
ENABLING REAL-TIME NEURAL RECOVERY FOR CLOUD GAMING ON MOBILE DEVICES

Zhaoyuan He¹, Yifan Yang², Shuoze Li¹, Diyuan Dai¹, Lili Qiu^{1,2}, Yuqing Yang²

¹Department of Computer Science, The University of Texas at Austin, Austin, TX, USA

²Microsoft Research Asia Shanghai, Shanghai, P.R.China

ABSTRACT

Cloud gaming is a multi-billion dollar industry. A client in cloud gaming sends its movement to the game server on the Internet, which renders and transmits the resulting video back. In order to provide a good gaming experience, a latency below 80 ms is required. This means that video rendering, encoding, transmission, decoding, and display have to finish within that time frame, which is especially challenging to achieve due to server overload, network congestion, and losses. In this paper, we propose a new method for recovering lost or corrupted video frames in cloud gaming. Unlike traditional video frame recovery, our approach uses game states to significantly enhance recovery accuracy and utilizes partially decoded frames to recover lost portions. We develop a holistic system that consists of (i) efficiently extracting game states, (ii) modifying H.264 video decoder to generate a mask to indicate which portions of video frames need recovery, and (iii) designing a novel neural network to recover either complete or partial video frames. Our approach is extensively evaluated using iPhone 12 and laptop implementations, and we demonstrate the utility of game states in the game video recovery and the effectiveness of our overall design.

1 Introduction

Motivation: The cloud gaming market has been experiencing a rapid surge in popularity, with the global cloud gaming market size projected to grow at a CAGR of 64.1% and reach \$14.01 billion by 2027 [13]. In cloud gaming, a player’s input is transmitted to a remote game server on the Internet, which renders and sends back the resulting video for display on the client side. To provide a satisfactory gaming experience, high bandwidth and low latency are required. For instance, GeForce NOW requires at least 15Mbps for 720p (25Mbps for 1080p) and below 80ms latency (40ms for the best experience) [21]. However, it is challenging to maintain a high throughput throughout the game session due to fluctuations in Internet performance and server load. If network congestion or server overload occurs, the video frames may not be delivered in time, leading to a disruption in the player’s experience.

While TCP retransmission can recover packet losses, its effectiveness is limited in cloud gaming due to the strict real-time requirements. Retransmissions are often too late to be useful, which is why most cloud gaming platforms opt for UDP for faster video transmission [16]. Forward error correction (FEC) can recover losses without adding extra delay, but it is challenging to predict the packet loss rate in advance and properly adjust the amount of FEC to add. Moreover, FEC is expensive: as reported in [35], WebRTC increases the FEC to 50% of original video data under 4% packet loss, and to 80% under 10% packet loss. There are also various proposals to enhance video codecs, but it is challenging to deploy a new codec on a large scale. Therefore, to maximize our impact, we seek an approach that can recover losses without adding significant delay, overhead, or modifying video codecs.

Our approach: Motivated by the observation, we explore how to recover video frame(s) on the client side whenever the client does not receive them in time. Video prediction and error concealment have been extensively researched in various contexts (*e.g.*, [44, 62, 75, 47, 18, 48, 49]), but in cloud gaming, the client possesses game state information that includes crucial details such as the shapes, sizes, colors, orientations, positions, and movements of game objects. This information can be highly beneficial for video recovery purposes.

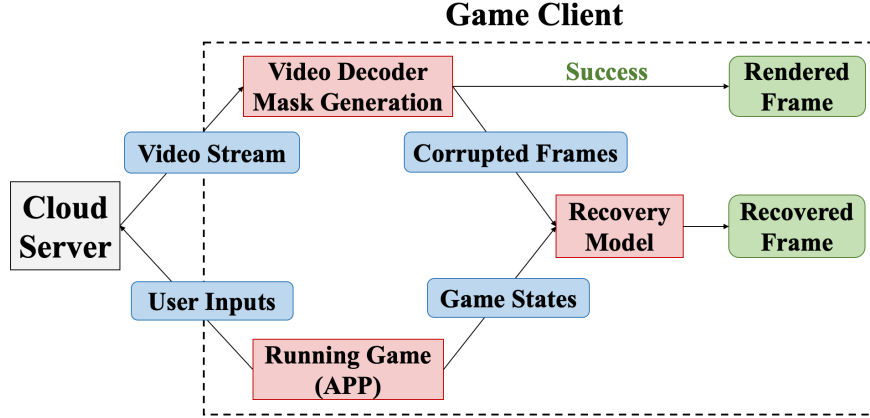


Figure 1: Overview of our video recovery system.

To leverage game state information for video recovery, there are three critical research questions that need to be addressed: (i) how to efficiently extract and represent the game states, (ii) how to effectively utilize the game states for video recovery, and (iii) to what extent can game states assist in video recovery.

To answer these questions, we develop a novel video recovery system shown in Figure 1. First, the game client can efficiently extract game states from a running game app without rendering the whole frame. We only need to render foreground interactions and deformable objects. We create a Compute Shader that transforms the 3D vertices of each visible game object into a 2D screen. To speed up game state extraction, we preload all objects’ vertices into GPU at the beginning of games and create an array to indicate whether game objects exist in the current frame, thereby minimizing the overhead of uploading information from CPU to GPU. We further experiment with different game state representations, sizes, and resolutions to identify the appropriate configuration that balances the speed and accuracy. Note that the game state can also be extracted at the server and transmitted reliably to the client.

We then modify the H.264 video decoder using FFmpeg to generate a mask that indicates which parts of a video frame have decoding errors and require recovery. The game states and corrupted frames are fed into our recovery model for video recovery.

Next, we design a novel neural network that can leverage game states to recover both complete and partial video frames. We first compute the optical flow between the current and previous game states and use it to warp the previous RGB frame to the current one. To improve the image quality, enhancement and inpainting modules are included to not only align pixels but also change colors and generate new content to better restore the image.

In this paper, we focus on a hybrid system that splits the rendering between clients and cloud servers. We present a novel design that systematically implements our recovery model on both iPhone 12 and laptop devices, enabling the support of 30 FPS cloud gaming. Through extensive evaluations under diverse network conditions, we demonstrate significant improvements in recovered frames, achieving up to 9.7 dB PSNR. Furthermore, our approach effectively leverages game state information, resulting in a remarkable enhancement of up to 5.4 dB PSNR compared to schemes that do not utilize game states. To the best of our knowledge, this work is the first to exploit game state information for cloud game video recovery, showcasing a considerable boost in video quality for real-time mobile gaming. By demonstrating the feasibility of deep learning-based video frame recovery on mobile devices, our work paves the way for seamless and uninterrupted gaming experiences despite network losses. To optimize client resource usage, game states can be extracted on the server side and reliably transmitted using TCP, with minimal transmission overhead due to their compact size of 8 KB. We expect this work to inspire further advancements in efficiency, ultimately contributing to the improvement of cloud gaming performance on mobile devices.

2 Related Work

We classify existing work into the following three areas: (i) cloud gaming systems, (ii) video streaming, and (iii) video recovery.

Cloud gaming systems: [6] provides a nice survey of cloud gaming research. There have been lots of works on optimizing cloud gaming systems, including virtual machine placement [23, 22], distributed game engines [4], GPU

sharing [45, 74], cloud scheduling [61], and resource allocation [40, 17, 38]. Some works [19, 64, 65, 2] leverage forward error correction (FEC) to protect game frames from losses, but FEC incurs significant overhead [35], which may make more frames miss their 33ms deadline for 30FPS games under a highly fluctuating network. Outatime [37] renders speculative frames one RTT in advance. Furion [34] employs a cooperative renderer architecture that renders foreground interactions locally on the phone while prefetching pre-rendered frames from servers to reduce delay. Game engine information has been used to speed up the motion estimation in video encoding H.264/AVC [50]. Chen *et al.* [8] use collaborative rendering, progressive meshes, and 3D image warping to dynamically adapt image quality.

Video streaming: To accommodate fluctuation in network performance, existing video streaming systems implement dynamic video rate adaptation. Many rate adaptation schemes have been proposed (*e.g.*, QDASH [41], FESTIVE [28], client-side buffer-based adaptation [55], [24] and QAVA [10]). [26] adapts the rate based on buffer occupancy. [70] develops a model predictive control (MPC) based on buffer occupancy and throughput estimation. [25] develops rate adaptation based on deep reinforcement learning. To enhance the performance, several works improve the throughput prediction by exploiting correlation between video sessions (*e.g.*, CFA [27] and CS2P [52]) or using ML approaches (*e.g.*, [39, 7]).

There has been a lot of work on video delivery over LTE (*e.g.*, [36, 53]). Due to the recent deployment of 5G, video streaming over 5G has attracted increasing interest. 5G poses more challenges due to its larger fluctuation and unpredictability. [42] empirically compares several adaptive bit rate algorithms in 5G networks and reports 3.7% to 259.5% higher stall time than 4G/LTE.

Neural-enhanced video streaming has been well studied (*e.g.* NAS [68], LiveNAS [31], NEMO [67], NeuroScaler [69]). These approaches employ super-resolution models to enhance low-resolution frames to high-resolution either on clients or media servers, aiming to enhance transmission efficiency. Different from these works, our work specifically addresses video recovery for cloud gaming, which presents a greater challenge due to the stringent real-time demands typically associated with gaming. In contrast to merely enhancing existing frames, video recovery in gaming involves generating new content instead of enhancing individual pixels.

Video recovery: We classify the work of video recovery into two areas: video prediction and video error concealment. Many interesting algorithms have been proposed for video prediction. Several deep learning architectures have been used for video prediction, such as convolutional networks (*e.g.*, [62, 60, 56, 1]), recurrent networks (*e.g.*, [75, 54]), and generative networks. Among them, GANs are particularly effective for generation tasks. However, GANs are typically designed to generate realistic images, which may not be necessarily similar to the next frame. [47] also learns transformations, such as pixel motion, to synthesize the next video frame from the previous ones.

Several other works utilize neural networks to realize video error concealment such that corrupted frames can be recovered from previous frames. [48] predicts optical flow from generated flows of past frames to reconstruct the degraded portion of the frame. [49] designs a capsule network framework to extract the decoded temporal dependencies, which are further combined with past frames and passed through a reconstruction network to perform motion-compensated error concealment.

Summary: Our work differs from the existing work as follows: (i) our work is the first one that extracts and leverages the game state for complete or partial video frame recovery and demonstrates significant benefits of game states, and (ii) unlike the existing work, which focuses only on the video reconstruction accuracy, our system accurately recovers videos in real-time on mobile devices.

3 Motivation

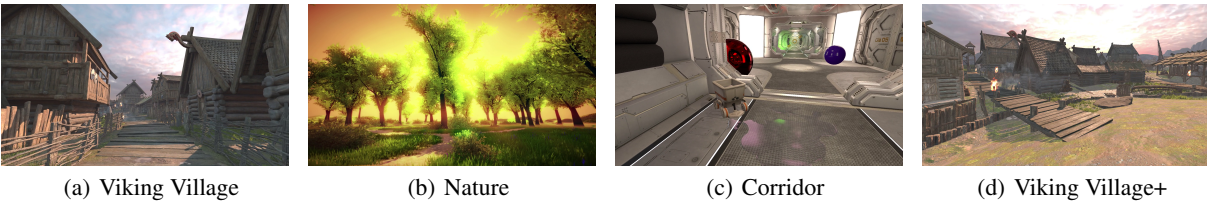


Figure 2: High-quality Unity games.

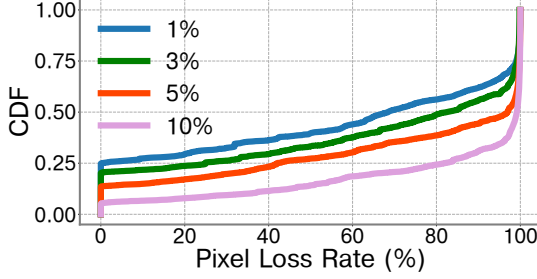


Figure 3: Average pixel loss rate of each frame under different network loss rates.

Machine	Game Name	FPS
iPhone 12	Viking Village	20
	Nature	23
	Corridor	17
Laptop	Viking Village+	18

Table 1: Frame rate when running different games

3.1 Local Rendering

Network performance fluctuates widely [53, 36, 42]. When the network condition degrades, a natural solution is to perform local rendering on the client side. To assess the feasibility of this approach, we measure the resource usage and resulting frame rate when rendering on the two following local devices: (i) iPhone 12: Apple A14 Bionic Chipset, Hexa-core (2x3.1 GHz Firestorm + 4x1.8 GHz Icestorm) CPU and Apple GPU (4-core graphics), and (ii) laptop: Intel(R) Core(TM) i5-9300H at 2.40GHz CPU and GeForce GTX 1650 (Mobile) GPU. With over 94% of U.S. iPhone purchases in Q1 2023 being iPhone 12 and higher versions [12], it can be inferred that most users’ smartphones should match or exceed the performance of the iPhone 12. We consider the following three games in our measurements: Viking Village [59], Corridor [14] and Nature [43]. They are high-quality virtual-world Unity apps with complex and realistic environments as shown in Figure 2. We use them for our experiments because they are originally designed for high-end PCs.

Table 1 shows that the first three games achieve only 17-23 frames per second (FPS) on the iPhone 12, which is insufficient to support a typical requirement of 30 FPS. The laptop has a more powerful CPU and GPU, and can achieve over 30FPS for these three games. However, as the games get more complex, local rendering can also become infeasible even for the laptop. For validation, we build a larger game based on Viking Village by increasing the game area and adding more game objects to the scene. We call the larger game Viking Village+, as shown in Figure 2(d). The laptop can only achieve 18 FPS for Viking Village+.

These results show that existing local rendering is often infeasible and motivates us to seek alternatives to recover corrupted frames due to prolonged network or server delay.

3.2 Video Prediction

Video prediction has been well studied and can help us recover lost frames. Many state-of-art video prediction models are too heavy to perform inference on the laptop in real-time (*e.g.*, within 33ms). For example, CrevNet [72] and PreRNN+ [63] take 600ms and 3s to predict 1080p frames on the laptop, respectively.

An alternate way to predict frames is to calculate the optical flow between the last two frames and warp the previous frame using the optical flow. Unfortunately, state-of-art optical flow models are not fast enough to perform real-time inference for 1080p videos. For example, it takes SPyNet [46] 250ms to compute the optical flow between two consecutive frames on the laptop.

It is challenging to accurately predict video frames due to uncertainties in future events. For example, CrevNet [72] achieves 0.49 SSIM and 19.2dB PSNR for game video prediction. Such accuracy is insufficient to support a satisfactory gaming experience. Meanwhile, we observe that video frames from a game are rendered based on the game states. This gives us an opportunity to leverage the game states to significantly improve the accuracy of video prediction.

3.3 Partial Recovery

To understand how packet losses affect the video frame delivery, we conduct the following measurement. We set up a video streaming session and add cross traffic to the network to incur around 1%, 3%, 5%, and 10% average packet loss rates. Figure 3 plots the fraction of corrupted pixels in video frames under various packet loss rates. As we can see, 25% frames are completely lost and 50% frames are partially corrupted after decoding under the 1% packet loss rate. The numbers are even higher under a higher loss rate. Note that when reference frames are lost, all frames that

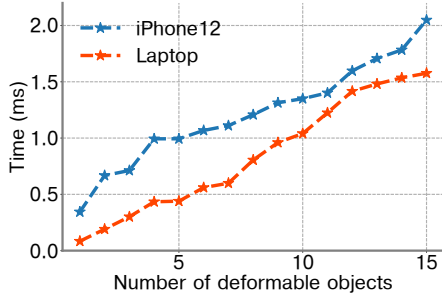


Figure 4: Local rendering time for deformable objects.

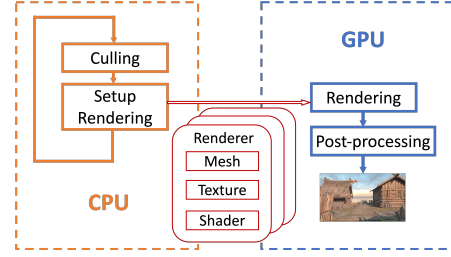


Figure 5: Simplified Rendering Process in Unity

depend on them are lost, as well. These results suggest that it is necessary to develop a video recovery approach that can recover both partial frame loss and complete frame loss.

3.4 Foreground Interactions and Deformable Objects

Furion [34] provides an insight that a game frame usually consists of foreground interactions and a background environment. The background environment is fairly predictable since it is incrementally updated as objects or camera moves in the game world. However, it has a heavier rendering load due to rich details and complex textures, so it is recommended to render and transmit from the server. The foreground interactions are more lightweight but unpredictable and hence are suited for rendering on the client side.

We preload game objects to GPU and use our model to recover the frames that are partially or completely lost. This strategy works for rigid objects since it requires that the vertices remain the same throughout the game. If an object is deformable, we have to upload its updated vertices to the GPU again. The overhead increases with the number of deformable objects. To avoid such overhead, we also follow the cooperative rendering strategy in Furion to leverage local machine’s GPU to render the deformable objects. Figure 4 shows that the time for rendering up to 15 deformable objects is around 2ms and 1.5ms on the iPhone 12 and laptop, respectively, which is acceptable for our 30 FPS system. It suggests that we can classify the objects into rigid vs. deformable, recover the rigid objects using our model, and apply local rendering for deformable objects.

3.5 Summary

In this section, we show that it is challenging to perform local rendering or video recovery in real time and the current game video prediction accuracy is insufficient. Moreover, we find that it is common to receive partially corrupted frames when packet loss happens. These observations motivate us to develop a video recovery algorithm to recover both partially corrupted frames and completely lost frames. We follow the cooperative rendering strategy shown in Furion [34] to leverage local machine’s GPU to render foreground interactions and deformable objects.

4 Extract and Represent Game States

In this section, we present our approach to extracting and representing the game states. We use the games developed from Unity [57], but our approach is general and can potentially support other game engines. Below we first provide a brief overview of Unity and then describe our game state extraction.

4.1 Background

Unity [57] is a cross-platform game engine developed by Unity Technologies. It is primarily used to develop video games and simulations. At a high level, the Unity rendering pipeline consists of culling, rendering, and post-processing [58]. Figure 5 shows a simplified rendering process in Unity.

Culling: For each frame, a camera performs frustum culling to remove renderers that fall outside the camera’s view. Occlusion culling further removes the occluded objects. Both frustum culling and occlusion culling remove the need of rendering unnecessary objects and enhance efficiency. Then the CPU will upload visible renderers, camera’s matrices, and others to the GPU for rendering.

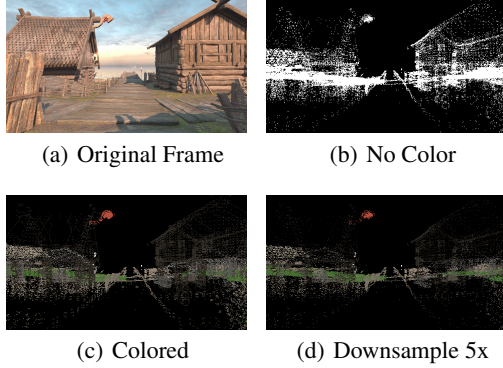


Figure 6: An example of game states.

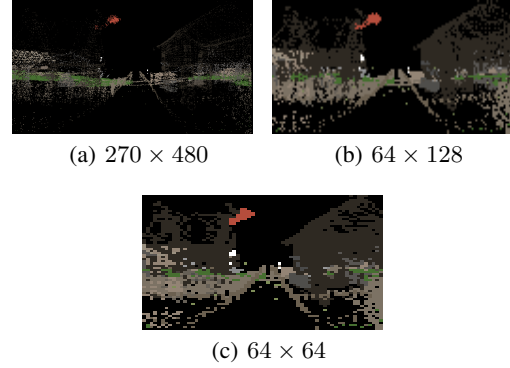


Figure 7: Game states in different resolutions.

Rendering: The rendering step involves creating geometry, adding lighting effects, and projecting the 3D environment onto the 2D screen based on the camera configuration. A renderer consists of meshes, textures, and shaders. A mesh describes the geometry of a game object and is represented using vertices and multiple triangle arrays. Each game object has at least one texture, which determines its color and transparency. The shader is a program that computes the color of each pixel according to the lighting and material.

Post-processing: Unity offers post-processing effects, such as blurring the background and moving objects, balancing colors around white areas, adding fog effects, etc. They are used to create specialized visual effects.

4.2 Game States

We extract the game states from the running game app, which include game objects’ locations, speeds, rotations, sizes, etc. The game states along with the previous frames can be used together to improve the game video prediction.

Algorithm 1 shows the pseudo-code for our game state extraction. On the CPU side, we first extract all renderers and then mimic frustum culling by checking each object’s bounding box against the frustum of the camera. Any renderers whose bounds are not visible will be skipped. Then we send the camera’s Projection (P), View (V), and object’s Transform (T) matrices, along with all visible vertices to the GPU. T transforms from the object’s local space to the global space, V converts the global space to the camera view, and P specifies how the camera maps a 3D world onto a 2D image. Different from the CPU processing in Figure 5, we gather and send only the above information to GPU because they can completely capture the states for each frame. In this way, we can extract the game states without rendering the whole game frame, thereby avoiding much overhead on the client side.

Compute shaders are programs running on the GPU outside the rendering pipeline. They can be used for massively parallel GPU computation. Since Unity does not provide APIs to access the intermediate results, we derive the game states by developing our own compute shaders to transform the 3D vertices of each visible object onto a 2D screen. To do so, we calculate the Model View Projection (MVP) matrix based on the camera’s Projection (P), View (V), and object’s Transform (T) matrix using $MVP_{f,i} = P_f \times V_f \times T_{f,i}$ where f is the frame index and i is the game object index. MVP converts each object from the local space to the clip space. Then we specify the 2D screen size to perform a viewport transform and generate the final game states on the 2D screen. Figure 6(a) and

Algorithm 1 Game States Extraction

```

1: CPU:
2: for frame  $f = 1, 2, \dots$  do
3:   for object  $i = 1, 2, \dots, N$  do
4:     Check the bounding box against the frustum of the camera to skip invisible
       objects
5:   end for
6:   Send  $P, V, T$  matrix and all visible vertices to the Compute Shader running
       on GPU
7: end for
8: GPU:
9: for all vertices in parallel do
10:  Perform  $MVP$  matrix multiplication
11:  Transform each 3D vertex from the local space to the 2D screen space
12:  Filter out the points outside the 2D screen
13: end for
14: Send the game states back to CPU
    
```

6(b) are a RGB frame and the game state at a resolution of 270×480 .

Downsampling	$T_{multiplication}$		Size	$T_{GPU \rightarrow CPU}$	
	iPhone 12	Laptop		iPhone 12	Laptop
1×	12.8ms	4.0ms	270×480	1.5ms	0.2ms
2×	7.9ms	2.5ms	64×128	0.8ms	0.1ms
5×	4.3ms	1.3ms	64×64	0.6ms	0.08ms
10×	3.6ms	1.1ms			

 Table 2: $T_{multiplication}$ with different downsampling ratios and $T_{GPU \rightarrow CPU}$ with different sizes

As mentioned above, game state extraction involves the following steps: (i) perform culling, (ii) upload visible vertices of game objects from CPU to GPU, (iii) perform the matrix multiplication in parallel, and (iv) download the game states from GPU to CPU. Equation 1 and 2 show the time for generating 270×480 game states in Viking Village on the iPhone 12 and laptop. This is even slower than performing local rendering, which is not acceptable.

$$T_{gs_iphone12} = T_{culling} + T_{CPU \rightarrow GPU} + T_{multiplication} + T_{GPU \rightarrow CPU} \quad (1)$$

$(435.8ms) \quad (1.5ms) \quad (420ms) \quad (12.8ms) \quad (1.5ms)$

$$T_{gs_laptop} = T_{culling} + T_{CPU \rightarrow GPU} + T_{multiplication} + T_{GPU \rightarrow CPU} \quad (2)$$

$(237.5ms) \quad (3.3ms) \quad (230ms) \quad (4ms) \quad (0.2ms)$

4.3 Speed-up Game State Extraction

To reduce the latency, we observe that uploading vertices from the CPU to the GPU is the most time-consuming since it involves uploading several million 3D vertices. To address this issue, we find that the vertices of game objects remain the same in the local space. Whenever the camera or game object moves, we just need to let the Computer Shader know whether the game object exists in the current frame and how the MVP matrix changes. Therefore, we preload all objects' vertices into GPU at the beginning of the game. We create an array to indicate whether a game object exists in the current frame. We finally pass the array along with the P , V , and T matrices to the Compute Shader for matrix multiplication, thereby reducing $T_{CPU \rightarrow GPU}$ to 0.2ms and 0.08ms on the iPhone 12 and the laptop, respectively. The total size of all game objects' vertices is around 200MB in Viking Village and 630MB in Viking Village+, which can fit into GPU's VRAM on the iPhone 12 and the laptop.

4.4 Game State Representation

Colored game states: Colored game states give richer information and are likely to help video frame prediction. As an example, Figure 6(b) and 6(c) show a gray-scale game state and a colored one. We can more easily see different objects from the colored game state. However, the number of I/O operations increases with the colored game state since the RGB frame requires 3 channels whereas the gray-scale has only 1 channel. For each channel, a pixel value is represented as a 4-byte floating number in Unity. Using 3 channels increases $T_{GPU \rightarrow CPU}$ from 1.5ms to 4.2ms on the iPhone 12. To avoid the delay increase, we build a HashMap to store the color of all game objects at the beginning of the game. In this way, the values of the game states sent back from GPU are colored indices rather than real pixels. The CPU will look for the corresponding colors from the HashMap and rebuild the game states with RGB channels without extra cost. Note that the HashMap has a fixed number of game objects and yields a negligible increase in memory size. For example, Viking Village has around 1,500 objects and yields only 4.4KB memory increase. Moreover, we leverage the depth information of 3D vertices to filter out the farther vertex if two vertices from different game objects are mapped to the same point on the 2D screen.

Game state resolution: To reduce the matrix multiplication time on GPU, we downsample the vertices in the game states. We try different downsampling ratios and measure the computation time. Table 2 shows that downsampling by a factor of 2, 5, and 10 reduces $T_{multiplication}$ to 7.9ms, 4.3ms, and 3.6ms on the iPhone 12, and reduces to 2.5ms, 1.3ms, and 1.1ms on the laptop, respectively. Figure 6(d) shows an example of game states with 5× downsampling ratio. In order to reduce $T_{GPU \rightarrow CPU}$, we also vary the resolution of the game states. Table 2 shows that reducing the frame size from 270×480 to 64×128 and 64×64 reduces $T_{GPU \rightarrow CPU}$ to 0.8ms and 0.6ms on the iPhone 12, and reduces to 0.1ms and 0.08ms on the laptop. Figure 7 shows examples of game state frames using different resolutions. We can still clearly see the objects in all resolutions. The game state frames are plotted in the same size just for visualization, and we use actual resolution for inference.



Figure 8: An example of a corrupted frame and the corresponding mask.

4.5 Summary

Our optimization reduces the latency of game state extraction to Equation 3 and 4.

$$T_{gs_iphone12} = T_{culling} + T_{CPU \rightarrow GPU} + T_{multiplication} + T_{GPU \rightarrow CPU} \quad (3)$$

$(5.9-16ms) \quad (1.5ms) \quad (0.2ms) \quad (3.6-12.8ms) \quad (0.6-1.5ms)$

$$T_{gs_laptop} = T_{culling} + T_{CPU \rightarrow GPU} + T_{multiplication} + T_{GPU \rightarrow CPU} \quad (4)$$

$(4.5-7.6ms) \quad (3.3ms) \quad (0.08ms) \quad (1.1-4ms) \quad (0.08-0.2ms)$

5 Mask Generation

As the network performance degrades, part of video streams might be lost or corrupted. In this case, the video decoder will generate a partially corrupted frame on the client side. It is necessary to know which part of the frame is corrupted so that our recovery model can recover that part.

As we know, a key frame (I-frame) is a complete video frame, while a P-frame and B-frame contain the change from the reference frame. Therefore a frame can have decoding errors either because a portion of packets corresponding to the frame has corruption or because its reference frame is corrupted. In order to properly generate a mask that indicates which parts of the frame are corrupted, we need to understand the video codec.

The widespread H.264 codec is used by both Stadia and GeForce Now, so we focus on H.264 in this paper. FFmpeg, an open-source video codec, is used for our implementation. In the H.264 video stream, a coded picture consists of a number of macroblocks. They have three types. I macroblocks are predicted using intra prediction from decoded samples. P macroblocks are predicted using inter prediction from its reference frame. B macroblocks perform similar decoding steps to P macroblocks but are predicted from one or two reference frames. All macroblocks range from 4×4 to 16×16 .

The H.264 decoder will not continue to decode the subsequent macroblocks if previous ones are missing or corrupted, thereby giving us an accurate position indicating which macroblocks are corrupted. The minimum size of sub-macroblocks is 4×4 and we can always get their reference blocks from inter or intra prediction during decoding, so we generate a mask to indicate whether each sub-macroblock can be decoded correctly. When generating the mask, we take into account both the macroblock itself and its reference block. Figure 8 shows an example of a corrupted frame and its mask. In the mask, the white color denotes a correctly decoded part while the black color denotes a corrupted part.

With the mask, we can leverage partially decoded frames for video recovery. It incurs a negligible overhead because we only use intermediate variables and do not require additional computation during the decoding. The mask is a gray-scale array that takes around 2MB of memory. The delta frame might be a few frames away from its reference frame, so we need to cache several masks (*e.g.*, 10) in the memory for future reference.

6 Video Recovery Model

A natural way to recover a video frame is to use the previous frames. There have been lots of existing works in this direction (*e.g.*, [73, 30, 44]). In cloud gaming, we can further leverage the current game states in addition to the previous video frames to improve the performance since the game states contain important information regarding the current objects' shapes, sizes, colors, orientations, positions, movements, etc.

Game state changes strongly correlate with RGB frames (from Unity's rendering logic), so they help our network to learn the mapping to RGB space optical flow. Our intuition is that the pixel-wise shifting O_S^t between the two game

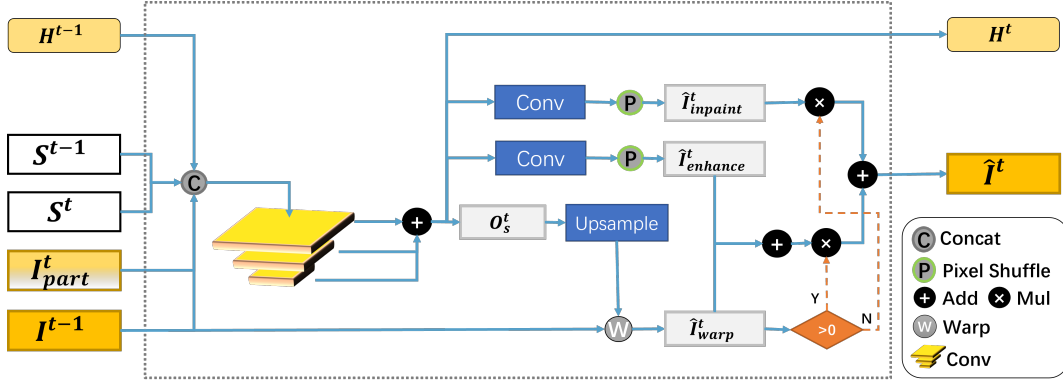


Figure 9: Model architecture diagram.

states S^{t-1} and S^t at time t is similar to O_s^t between the corresponding two frames I^{t-1} and I^t . Therefore, we can first compute O_s^t between the current and previous game states, and use it to warp the previous frame I^{t-1} to predict the current one I^t . That is, we compute $O_s^t = \mathcal{O}(S^{t-1}, S^t)$ and $\hat{I}^t = \mathcal{W}(I^{t-1}, O_s^t)$, where $\mathcal{O}()$ denotes the optical flow and \mathcal{W} denotes warping.

6.1 Estimating Optical Flow

The optical flow captures the movement of the brightness pattern and approximates the motion field. Let $u(x, y)$ and $v(x, y)$ denote the 2D optical flow for a given point (x, y) in a video frame. Under the assumption of the "intensity constancy", we have $I(x + \Delta x, y + \Delta y, t + \Delta t) \approx I(x, y, t)$. Through a Taylor series expansion, $I(x + \Delta x, y + \Delta y, t + \Delta t) = I(x, y, t) + \frac{\delta I}{\delta x} \Delta x + \frac{\delta I}{\delta y} \Delta y + \frac{\delta I}{\delta t} \Delta t$. Hence we have $\Delta I v + I_t = 0$ where $v = (\Delta x, \Delta y)$ is the optical flow, $\Delta I = (I_x, I_y)$ is the spatial gradient, and I_t is the temporal gradient. By deriving ΔI and I_t from a pair of video frames, we get the optical flow v .

Optical flow can be estimated by phase correlation, block-based, differential methods, discrete optimization, and deep learning approaches. We choose SPyNet [46], one of the most widely used optical flow networks due to its high efficiency and accuracy.

Figure 9 shows our model architecture. We initialize the pyramidal convolution backbone with a SPyNet pre-trained on Sintel [5]. It uses the current game states S^t and the previous one S^{t-1} to capture optical flow. It then downsamples the input 5 times through a pyramid structure and accumulates the predicted optical flow layer by layer to get O_s^t .

6.2 Refining & Warping Using Optical Flow

The optical flow between the two consecutive game states can be used to warp the previous RGB frame to the current one. However, the optical flow between the two game states differs from the optical flow between the two corresponding RGB frames in the following way: (i) game states have a finite number of scatter points and their frames are more sparse, (ii) the movement of the scatter points are not the same as the movement of brightness patterns in RGB frames, and (iii) the resolution of game states is usually much lower than RGB frames for the sake of computational efficiency, so the resulting flow cannot be used directly for warping.

For the output optical flow O_s^t , we use bilinear interpolation and grid sample-based warping to create an aligned prediction \hat{I}_{warp}^t from the previous frame I^{t-1} . This fully differentiable process enables gradient propagation to optimize the optical flow network and produce accurate results.

6.3 Enhancement and Inpainting

Warp-based video frame prediction can only predict the visible content in the previous RGB frames, and cannot modify the color gap for the new frame or generate content that does not exist in previous frames. Therefore, we improve the optical flow network by adding the following inputs to enable the generation of new content: (i) previous frame I^{t-1} to add unavailable details in the game states, (ii) current partially decoded frame I_{part}^t as a reference to align the generated content to the received partial frame, and (iii) hidden state H^{t-1} , including historical information to make the generated frames temporally smooth.

After the pyramid network, we generate $\hat{\mathbf{I}}_{enhance}^t$ and $\hat{\mathbf{I}}_{inpaint}^t$ using two sets of convolutions as Figure 9 shows. We use pixel shuffle[51] to scale the feature map to the size of RGB frames. $\hat{\mathbf{I}}_{enhance}^t$ learns the gap from $\hat{\mathbf{I}}_{warp}^t$ to the ground truth to make the prediction more natural. It focuses on the meaningful content of the warped image and ignores the empty parts. $\hat{\mathbf{I}}_{inpaint}^t$ generates new content when warping cannot find reference in previous frames, so it is only responsible for the empty part of $\hat{\mathbf{I}}_{warp}^t$. The final prediction can be expressed as follows:

$$\hat{\mathbf{I}}^t = (\hat{\mathbf{I}}_{warp}^t + \hat{\mathbf{I}}_{enhance}^t) * M + \hat{\mathbf{I}}_{inpaint}^t * (1 - M)$$

where M is a bitmap and its value is 1 if $\hat{\mathbf{I}}_{warp}^t$ is not empty otherwise 0. Finally, we overwrite it with \mathbf{I}_{part}^t that has already been decoded.

We quantify the difference between the predicted and actual RGB frames using the following loss function: $\mathcal{L}^t = \mathcal{L}_{Pix}^t + \alpha \mathcal{L}_{distill}^t$. α is set to 0.1. $\mathcal{L}_{Pix}^t = \mathcal{C}(\hat{\mathbf{I}}^t, \mathbf{I}^t)$ and $\mathcal{C}(\hat{\mathbf{I}}^t, \mathbf{I}^t) = \sum_i^W \sum_j^H \sqrt{(\hat{\mathbf{I}}_{ij}^t - \mathbf{I}_{ij}^t)^2 + \epsilon^2}$ where $\hat{\mathbf{I}}^t$ and \mathbf{I}^t denote the actual and predicted frames at time t , respectively. W and H denote the width and length of the input video, and ϵ is a small constant set to $1e^{-12}$. We use Charbonnier loss [33] as the loss function \mathcal{C} . The Charbonnier loss is a differentiable variant of \mathcal{L}_1 distance, which is shown to perform well for generation tasks [3, 20, 15]. We also add a distillation loss[51, 32] $\mathcal{L}_{distill}^t = \mathcal{C}(\mathbf{O}_S^t, \mathbf{O}_{fix}^t)$ to the output optical flow \mathbf{O}_S^t . \mathbf{O}_{fix}^t comes from the output of the fixed SPynet we used for initialization in order to maintain the warping stability. We find that without this item, \mathbf{O}_S^t tends to spread the previous frame over the entire image to reduce loss, which renders the inpainting module ineffective.

7 System Implementation

Figure 1 shows our system architecture. The game client has a running game app to efficiently generate game states without rendering the whole game frame when users play the game. The video decoder is utilized to generate a mask to indicate which portions of video frames need recovery. The game states and corrupted frames are fed to our recovery model for video frame recovery. Our goal is to develop a system that can be easily applied to different games. Meanwhile, in order to satisfy the 30 FPS requirement, we need to keep the total processing time within 33ms. We also devise a strategy about when to run the recovery model and how to optimize video quality.

Easy to deploy: Our game states extraction is easy to deploy. We provide two scripts. The first one automatically identifies and preloads vertices into the GPU during initialization and transmits matrices for extracting game states for each frame. The second script uses a Compute Shader on the GPU to generate the game states. These scripts can be used for any new games without modification. Programmers simply need to attach the scripts as modules to the game’s main camera through the Unity UI. This can be done by double-clicking on the main camera and importing the script without understanding the game’s source code. Furthermore, we modify video codec to generate masks, which can be compiled into FFmpeg during video decoding.

Speeding up inference time: The inference time for our recovery model highly depends on the game state size. We choose the size of 64×128 because it gives us a good balance between delay and accuracy as shown in Section 8. Our target devices are iPhone 12 and laptop, which have different computational capabilities and we use different speedup methods on these devices.

Our neural recovery model is highly flexible and can support various feature map sizes as input to accommodate different hardware constraints. In order to generate the target output size, we apply an optical flow upsampling to the feature map with different upsampling rates to match the target output size. This allows us to freely choose the size of the feature map for generating optical flow, thus making efficient use of the device’s computational power.

We use CoreML as the model format on the iPhone 12 because it optimizes on-device performance for iOS by leveraging the CPU, GPU, and Neural Engine. Therefore, we convert pretrained recovery model from Pytorch to CoreML and it performs faster than ONNX, Pytorch Mobile, and TensorFlow Lite. However, we observe that the grid sample operation of warping runs slowly because it is not officially supported by GPU. To address the above issue, we leverage Metal Performance Shaders (MPS) to create a custom grid sample layer running on GPU. MPS is a framework with handy Metal compute kernels and CoreML uses it for model inference on GPU. It also provides us with many APIs to create a custom layer so that the grid sample is implemented with a GPU acceleration on the iPhone 12. In addition, we perform warping at a smaller scale of 270p instead of 1080p, thereby reducing the warping time from 29ms to 5ms. The lost texture details caused by the downsampling will be made up by the enhancement module in Section 6.3. To further reduce the inference time, we use FP16 precision for both inputs and model weights without performance degradation. The final inference time is 22ms on the iPhone 12.

	4G	5G	WiFi	LEO
Amount of traces	145	152	150	146
Avg. Duration (s)	320	390	300	300
Avg. Throughput (Mbps)	32.5	61.7	72.8	28.9
Avg. Loss rate (%)	3.2	2.3	0.9	9.4

Table 3: Network traces

Since our laptop runs Linux and has Nvidia GPU, we can use Pytorch with CUDA as the inference framework. To optimize the inference speed, we choose TVM [9], which uses compiler techniques to optimize model inference. TVM works well with Pytorch and provides us with a 50% inference time reduction. The final inference time on the laptop is $25ms$.

Scheduling recovery: A natural solution is to run video recovery upon a partial or complete loss of a video frame. However, this yields large delay since the client’s game state extraction and recovery can only happen after the current video frame times out. To reduce the delay, we prefer overlapping the client side game state extraction with the server side processing and network transmission. But this requires the client extract the game state without knowing whether the current video frame will arrive in time. To limit the client’s resource consumption and end-to-end delay, we let the client start game state extraction for a video frame if the previous video frame is lost since network losses are bursty according to both previous measurement studies [66, 71] and our own measurement. By analyzing the network traces shown in Table 3, we calculate the loss probability of the current frame conditioned on the previous frame being lost is around 95%.

End-to-end latency: With our system strategies, we can perform neural recovery without waiting for video packets received, so the recovery latency would be the sum of game states extraction runtime and model inference time. According to Section 4.5, we have a range of runtime for game states generation. On the iPhone 12, we choose the game state resolution of 64×128 and downsample it by $5\times$, resulting in $7ms$ for game states generation and a total latency of $29ms$. On the laptop, we do not downsample the game states and utilize a resolution of 270×480 , which leads to $5ms$ for game states extraction and a total latency of $30ms$.

The end-to-end latency in cloud gaming refers to the duration starting from when the user enters an input to when the resulting frame is displayed on the client device. Users can tolerate an end-to-end delay ranging from $80 - 150ms$ [21, 11, 65, 8] depending on game types, so we choose $80ms$ as the maximum latency budget. To ensure the latency with recovery less than the time budget, we set a timeout before executing video recovery. If the partially corrupted frame can be received and processed within the timeout, our system will perform video concealment to recover the frame. Otherwise, the video prediction will be executed to avoid passing the deadline.

8 Performance Evaluation

In this section, we first present the evaluation methodology and then describe the performance results.

8.1 Evaluation Methodology

Datasets and metrics: We use Viking Village [59], Nature [43], Corridor [14] on the iPhone 12, and Viking Village+ on the laptop. Each game video lasts around 5 mins and they are collected by different players. There are 50,000 training frames and 10,000 testing frames for each game. We quantify the quality of our recovered video frames using two widely used video quality metrics: SSIM and PSNR. Higher SSIM and PSNR values indicate better video quality.

Network traces: Table 3 shows the network traces we use. We measured the downlink throughput using *iperf* from an Azure server located in the central U.S. to a local client over the Internet, where we varied the wireless hop to use WiFi, 4G, and 5G networks. *iperf* generates TCP data streams and provides the number of retransmissions and throughput. We compute the packet loss rate by dividing the number of retransmissions by the total number of transmissions. The 4G and 5G traces include static and walking scenarios. We also move the local client randomly to add mobility to the WiFi traces. The low earth orbit (LEO) satellite network traces were collected from the StarLink network in January 2023 using a StarLink RV ground station in the west coast of U.S. under a static scenario. To measure the packet loss rate, we ping the server every $10ms$ and collect the average ping drop rate.

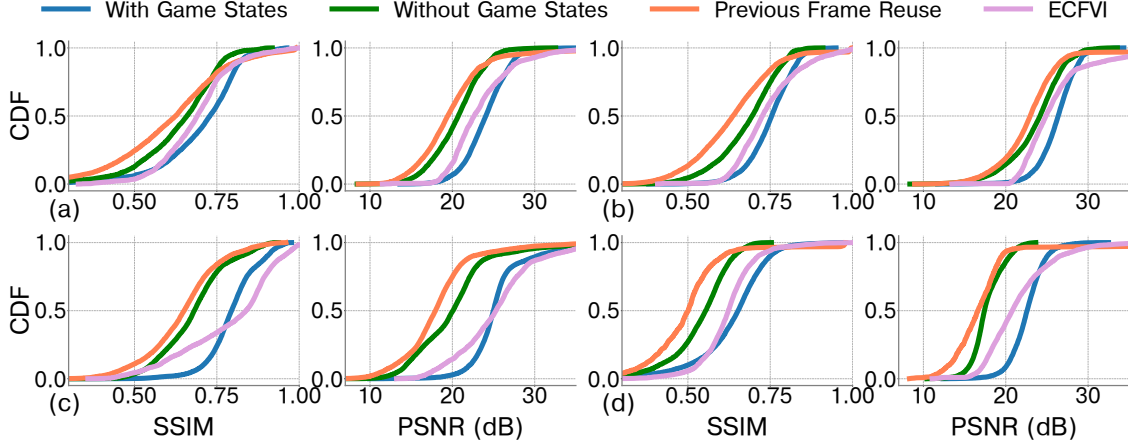


Figure 10: Performance results for different games. (a) Viking Village. (b) Nature. (c) Corridor. (d) Viking Village+

Evaluation strategies: We use the collected network traces to delay packets according to the timestamp recorded by the traces before sending them to the client. The client executes our system by decoding the video and recovering corrupted frames if needed. We compare the video recovery in two ways. First, we recover every frame assuming all previous frames are correctly received. Second, we recover the corrupted frame with previously rendered or recovered frames. In this case, the recovered frame will be fed to the model for the next frame recovery. These two strategies are complementary: the former focuses on the recovery for different frames while the latter focuses on the impact of realistic network losses. Note that we use network traces for evaluation so that all recovery algorithms are evaluated under the same loss conditions. We consider a lost packet when it misses its deadline where the deadline is determined based on the maximum tolerable end-to-end latency, i.e. 80ms, plus the inter-frame spacing (e.g., 33 ms for 30 FPS).

Implementation details: We use 100,000 iterations for all training rounds. We use an 8 GPU Tesla V100 machine with a batch size of 16. We set the learning rate to $1e^{-5}$, and use the cosine decay.

8.2 Performance Results

Impact of game states: We compare the following schemes for different games to analyze the impact of game states: (i) our method with game states, (ii) our method without game states, (iii) reusing the last frame as the recovered frame, and (iv) ECFVI [29], a state-of-the-art flow-guided video inpainting model. Note that here we assume the previous frames are received correctly. In (ii), we use the last two consecutive frames to replace the game states input in Figure 9 because they are usually used to get an optical flow in traditional video recovery algorithms. In (iv), ECFVI is limited to only restoring a 240p video frame. To enhance this, we introduce additional convolutional layers and incorporate a pixel shuffle layer to upscale from 240p to 1080p. This is trained using our dataset and evaluated at the same epoch as our model.

As shown in Figure 10, for Viking Village the improvements of (i) over (ii), (iii), and (iv) are 0.06, 0.1, and 0.012 in SSIM, respectively; 3.5dB, 4dB, and 0.7dB in PSNR, respectively; for Nature the corresponding improvements are 0.07, 0.12, and 0.008 in SSIM, respectively; 2.6dB, 3.1dB, and 0.4dB in PSNR, respectively; for Corridor the corresponding improvements are 0.11, 0.15, and 0.006 in SSIM, respectively; 5.6dB, 7.3dB, and 0.3dB in PSNR, respectively; for Viking Village+ the corresponding improvements are 0.09, 0.14, and 0.016 in SSIM, respectively, and 4.9dB, 5.6dB, and 0.9dB in PSNR, respectively.

We make the following observations. First, using game states significantly improves video quality over recovery without game states. Second, reusing previous frames only performs slightly worse than recovery without game states due to little change in consecutive video frames. Third, our light-weight video recovery model based on game states yield even better results than ECFVI, a much bigger model. We implement ECFVI using the same CoreML optimization and evaluate it on an Apple MacBook Air, as its high memory requirements prevent it from being deployed on an iPhone12. Therefore, we compare our implementation of ECFVI with our approach on Macbook Air and find ECFVI takes 6s to make an inference while our model takes only 18ms. This demonstrates the efficiency of our model and the benefit of incorporating game states.

Table 4 shows the recovered video quality of partially corrupted frames and completely lost frames. Since the former has a portion of the original frame, its recovered video quality is higher than that of the latter. Figure 11 shows

Recovery Type	Viking Village		Nature		Corridor	
	SSIM	PSNR	SSIM	PSNR	SSIM	PSNR
Partial	0.748	25.93 dB	0.798	28.74 dB	0.842	27.72 dB
Complete	0.692	24.07 dB	0.740	25.58 dB	0.771	24.94 dB

Table 4: Performance results for partially corrupted and completely lost frames

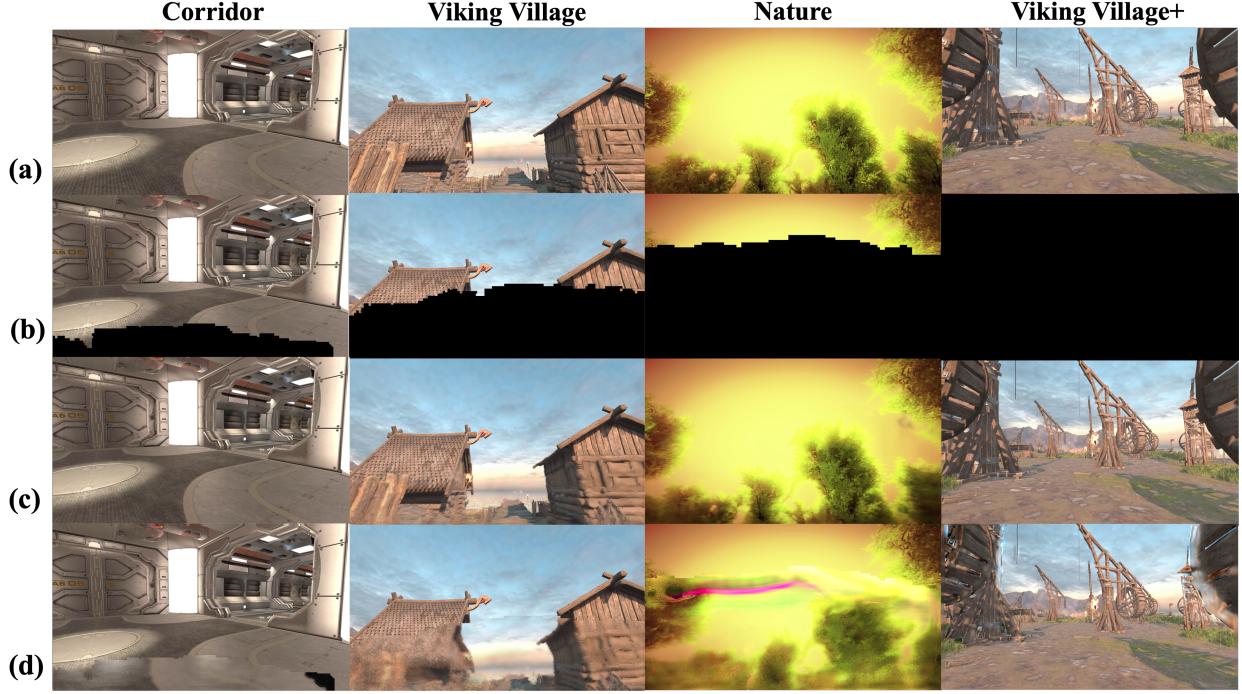


Figure 11: Visualizations analysis of our recovery model using different masks for different games. The first three columns are the results on the iPhone 12, and the last column is the result on the laptop. (a) Ground truth. (b) Partial frame extracted from the decoded frame using mask. (c) Recovered frame. (d) Recovered frame without game states.

the visualization of our recovery model using different masks for different games. It indicates that our method can effectively recover a partially corrupted frame and stitch it with the correct portion together for an accurate result. In comparison, it is difficult to predict the optical flow without game states such that the recovered frames are blurred and corrupted.

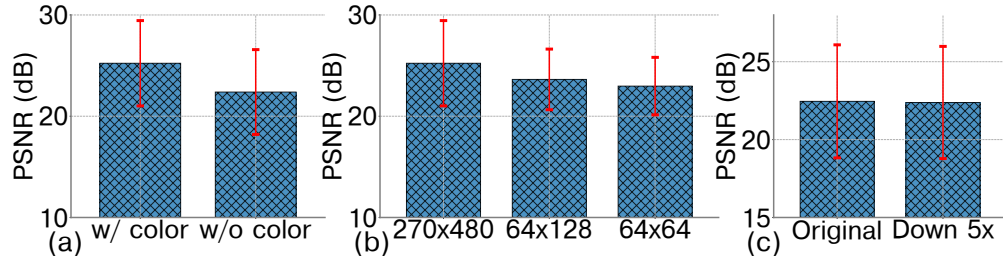


Figure 12: Performance results for game states. (a) w/ and w/o color. (b) different sizes. (c) different downsampling ratio.

Impact of game state representation: As shown in Figure 12, we study the impact of different game state representations in three dimensions: color, size, and downsampling ratio. For brevity, we only show PSNR results. We observe the followings: 1) After adding color, video quality has been improved by 2.9dB in PSNR as objects with different colors are better distinguished; 2) We compare three sizes of game states: 270×480 , 64×128 , and 64×64 .

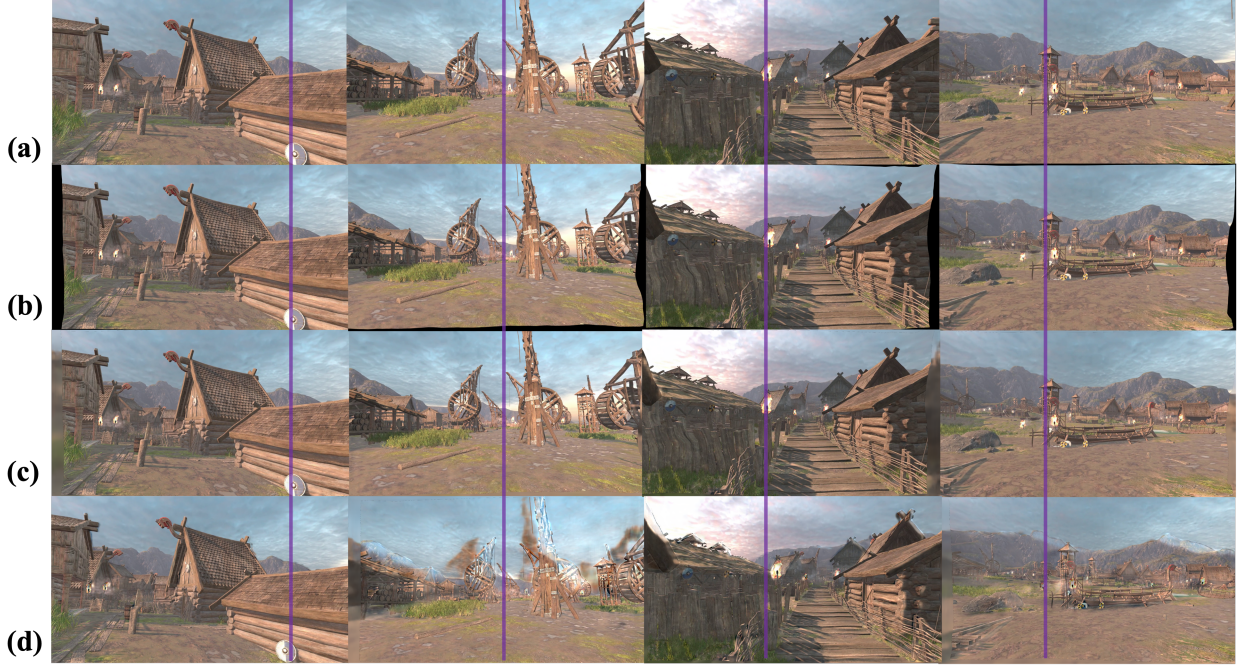


Figure 13: Visualizations analysis of enhancement and inpainting. Here shows the results of Viking Village+ on the laptop. A purple auxiliary line is added to reflect the alignment to the ground truth. We make a whole frame prediction. (a) Ground truth. (b) Warped result. (c) Recovered frame. (d) Recovered frame without game states.

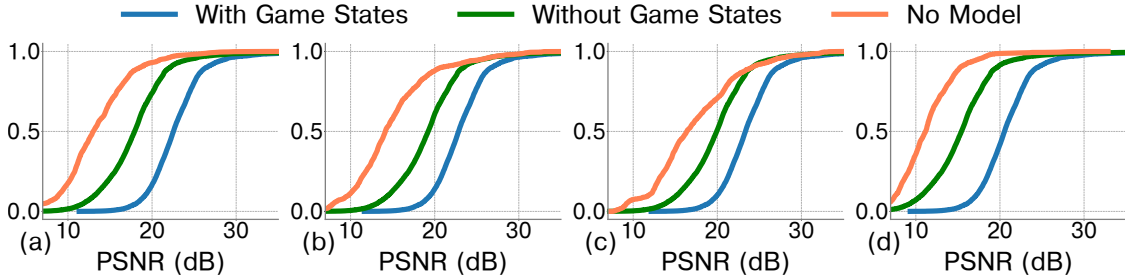


Figure 14: Performance results for different network traces. (a) 4G. (b) 5G. (c) WiFi. (d) LEO.

While larger sizes yield performance improvement, smaller game states can still yield acceptable performance. For example, using a 64×64 image to warp the previous frame achieves 23 dB PSNR. 3) Downsampling the vertices corresponding to the game objects by a factor of 5 has minimal effect on accuracy, while saving 66.4% and 67.5% of the computation time on the iPhone 12 and laptop.

Enhancement and Generation: As shown in Figure 13, row (b) shows the limitation of warping. Warping can only move pixels to achieve alignment but cannot generate new objects. For areas where no reference can be found from the previous frame, black borders appear. Row (c) shows that the black edge is reasonably filled in due to the inpainting module. The inpainting module restores the black area after warping, where the game states additionally serve as a hint for the generation because it contains the position information of all objects in the frame. Row (d) shows that the inaccurate flow causes the warping to be poorly aligned when no game states are applied. However, the enhancement module fixes the warped result such that the color of the inaccurately positioned object is suppressed and some correct colors are regenerated in the aligned area. Nevertheless, regeneration from scratch results in blurred and inaccurate predictions. Therefore, game states help to obtain a high-quality optical flow which is important to align features.

Impact of different network conditions: We further evaluate different network traces to analyze the impact of realistic network losses. We recover corrupted frames using previously rendered or recovered ones. In this case, the recovered frame will be fed to the model as an input for the next frame recovery. For better comparison, we compare

Network Traces	4G		5G		WiFi		LEO	
Recovery Type	Our	40% FEC	Our	35% FEC	Our	25% FEC	Our	70% FEC
Avg. pixel loss rate (%)	71	28	63	22	57	12	83	41
Avg. PSNR (dB)	31.65	29.01	33.53	31.58	37.51	36.8	27.95	23.26

Table 5: Comparison with forward error correction (FEC)

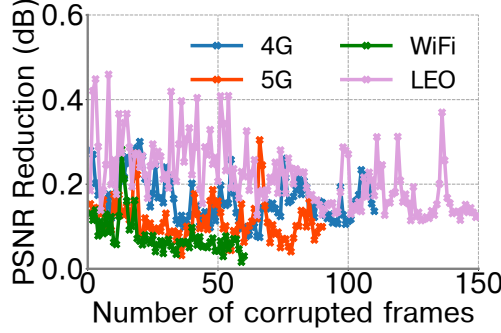


Figure 15: PSNR reduction with the number of consecutive corrupted frames.

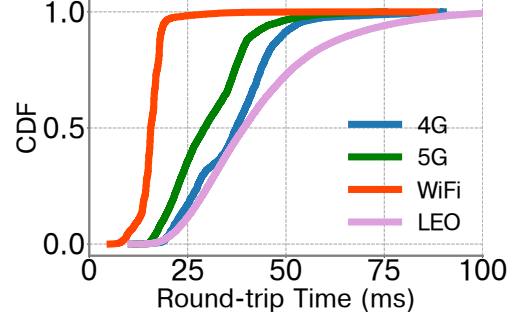


Figure 16: CDF of Round-trip Time (RTT) for different networks.

only the recovered frames. We consider three schemes: (i) recovery using game states, (ii) recovery without game states, and (iii) without our recovery model. Note that in (iii), our video decoder will reuse previous frames if the current frame is completely lost. Figure 14 shows the recovery performance for Viking Village under 4G, 5G, WiFi, and LEO networks. (i) out-performs (ii) by 4.8dB, 3.9dB, 3.7dB, and 5.4dB, respectively. (i) also improves (iii) by 9.1dB, 8.2dB, 6.4dB, and 9.7dB, respectively. As expected, (i) performs the best by using game states. The gain of (i) over (ii) is slightly improved compared with that in Figure 10(a) because (ii) uses the last two consecutive frames for recovery, so the recovery error will be more likely to accumulate. (iii) performs the worst because it cannot recover corrupted frames and its performance degrades fast under bursty packet losses. As shown in Table 3, the packet loss rate is 3.6%, 2.5%, 1.1%, and 9.4% for 4G, 5G, WiFi, and LEO traces, respectively. We observe that the overall PSNR degrades as the loss rate increases across different traces. Recovering using game states achieves a larger gain over the others as the loss rate increases due to fast error accumulation without game states.

Impact of scheduling recovery: We let the client start extracting game states for a video frame if the previous frame is lost or misses its deadline. In this way, video recovery is executed using the most recently rendered frame. So, if a frame A is the first missed frame, the subsequent frame will be recovered using A’s predecessor. The game state extraction for both A’s successor and predecessor occur simultaneously since we retain the user’s previous inputs in cache. On the iPhone12, this parallel extraction results in a 0.8ms increase in game state extraction time, which is negligible. We evaluate the impact of this method over different networks, especially during long burst of frame losses. Figure 15 plots the PSNR reduction along with the average number of consecutive corrupted frames for different networks. The average number of consecutive corrupted frames is 113, 89, 62, and 150 for 4G, 5G, WiFi, and LEO networks, respectively. Correspondingly, the average PSNR is reduced by only 0.17dB, 0.13dB, 0.06dB, and 0.26dB. The minimal drop in quality is largely attributed to the usage of game states, which offer significant details about the corrupted frame for recovery. It also benefits from our enhancement and inpainting module, which effectively corrects inaccurate warped pixels. Note that if a portion of a video frame is received correctly, we can use the received pixels to replace the predicted pixels.

Comparison with FEC: Table 5 compares average pixel loss rate and PSNR between our approach and oracle FEC, which knows the network loss rates in advance. To prevent packet loss, 40%, 35%, 25%, and 70% FEC are used in 4G, 5G, WiFi, and LEO network traces, respectively. However, due to extra FEC transmissions, some frames may not be delivered within 33ms deadline, resulting in frame losses. In comparison, our approach achieves higher video quality over FEC: it improves PSNR by 0.7-4.7dB and incurs less transmission overhead. Moreover, in practice it is challenging to realize the oracle FEC due to unpredictable network loss rate, and the performance gap between our approach and practical FEC is likely to be even larger.

Game Name	Server Render	Server Encode	Client Decode
Viking Village	3.6ms	4.5ms	7.2ms
Nature	2.9ms	4.3ms	7ms
Corridor	3.2ms	4.8ms	7.4ms
Viking Village+	8ms	5ms	7.6ms

Figure 17: Latency breakdown of server and client’s processing time when running different games

8.3 End-to-end latency

We evaluate the end-to-end latency when playing Viking Village, Nature, Corridor, and Viking Village+. Our game server operates on a desktop equipped with an AMD 12-Core Ryzen 9 5900 CPU, Nvidia GeForce RTX 3080 graphics card, and a 2TB SSD. Meanwhile, the client operates on an iPhone12, connected via 4G, 5G, WiFi, and LEO networks. We first evaluate the latency without the need of recovery and the components are as follows:

$$T_{non-recovery} = \underbrace{RTT}_{(15-42ms)} + \underbrace{T_{server_render}}_{(2.9-8ms)} + \underbrace{T_{server_encode}}_{(4.3-5ms)} + \underbrace{T_{tx}}_{(1.6-4ms)} + \underbrace{T_{client_decode}}_{(7-7.6ms)} \quad (5)$$

- RTT : This is a Round-trip time (RTT) involved in sending a user’s input and receiving the resulting video frame from the server (excluding the transmission time, which is accounted for in T_{tx}). Figure 16 illustrates the CDF of the observed RTTs. The average RTT is 36ms, 30ms, 15ms, and 42ms for 4G, 5G, WiFi, and LEO networks, respectively.
- T_{server_render} and T_{server_encode} : Upon receiving a user input from the client, the server processes and encodes the video frame using the H.264 codec. Table ?? illustrates that the server’s rendering time varies based on the game’s complexity, ranging from 2.9 – 8ms for the games we evaluated. For a fixed output resolution and encoding parameters, the encoding process takes 4.3 – 5ms, which has minimal fluctuation.
- T_{tx} : The duration required to transmit a frame from the game server to the client is influenced by the network bandwidth. Transmitting a 1080p video frame takes approximately 3.6ms over 4G, 1.9ms over 5G, 1.6ms over WiFi, and 4ms over LEO networks.
- T_{client_decode} : For the games we evaluated, as indicated in Table ??, the client on the iPhone12 processes and decodes an incoming video frame in 7 – 7.6ms.

The end-to-end latency may fluctuate depending on the network condition, system load, and the complexity of the game. When a video frame does not arrive before the deadline either due to a fluctuating delay or a lost frame, our system prompts the client to extract game state and execute video recovery for the next frame. As explained in Sec. 7, the end-to-end latency with recovery is as follows:

$$T_{recovery} = \underbrace{max}_{(<=80ms)}(\underbrace{min}_{(58ms)}(\underbrace{Timeout}_{(58ms)}, \underbrace{T_{non-recovery}}_{(30.8-66.6ms)}), \underbrace{T_{gs}}_{(7ms)}) + \underbrace{T_{inference}}_{(22ms)} \quad (6)$$

With an 80ms deadline budget and a model inference time of 22ms, the timeout can be adjusted to 58ms. The timer begins as soon as the user input is generated. Video recovery will be initiated either when the timer runs out or when a corrupted frame arrives. The game state extraction can be done in parallel with all steps except the model inference. It’s important to highlight that if pixels are received post-timeout but prior to the deadline, they can replace the recovered pixels. We also have the flexibility to vary the timeout for different latency budgets. The mechanism ensures our system’s capability to achieve real-time recovery for any missing or corrupted frame. Successfully recovered frames are stored locally and used for potential future recovery.

8.4 Resource Usage

In Sec. 4.3, the additional memory overhead for Viking Village and Viking Village+ is 200MB and 630MB, respectively, well below smartphones’ storage. Modern smartphones have a shared memory between the CPU and GPU. As the memory capacity of mobile devices continues to increase (e.g., 8GB, 16GB, 32GB), our memory requirement is quite affordable. With no frame loss, the server renders and transmits all video frames, similar to traditional approaches. In this scenario, iPhone 12’s CPU utilization is 35% and energy consumption is 0.05J per frame. Under 20% frame losses, the corresponding numbers are 41% and 0.06J per frame, and under 100% frame losses, they are 74% and 0.08J per

frame. Consequently, in the worst case when every frame needs recovery, the battery life decreases from 10.5 hours to 6.6 hours.

9 Conclusion

In this paper, we develop the first deep learning system for cloud gaming video recovery on mobile devices. Our system efficiently extracts and utilizes game states, generates a mask from H.264 video decoder to indicate which portions of frames need recovery, and develops a novel video recovery model to recover completely lost or partially corrupted frames to cope with server overload, network congestion, and losses in cloud gaming. Our extensive evaluation under diverse network conditions shows the effectiveness of our approach on mobile devices. We hope our work will inspire follow-up work to further enhance cloud gaming performance in challenging network environments.

References

- [1] S. Aigner and M. Korner. Futuregan: Anticipating the future “ frames of video sequences using spatio-temporal 3d convolutions in progressively growing autoencoder GANs. *arXiv:1810.01325*, 2018.
- [2] A. Alhilal, T. Braud, B. Han, and P. Hui. Nebula: Reliable low-latency video transmission for mobile cloud gaming. *arXiv preprint arXiv:2201.07738*, 2022.
- [3] J. T. Barron. A general and adaptive robust loss function. In *Proc. of CVPR*, 2019.
- [4] J. Bulman and P. Garraghan. A cloud gaming framework for dynamic graphical rendering towards achieving distributed game engines. In *HotCloud 20*, 2020.
- [5] D. J. Butler, J. Wulff, G. B. Stanley, and M. J. Black. A naturalistic open source movie for optical flow evaluation. In A. Fitzgibbon et al. (Eds.), editor, *ECCV*, Part IV, LNCS 7577, pages 611–625. Springer-Verlag, Oct. 2012.
- [6] W. Cai, R. Shea, C.-Y. Huang, K.-T. Chen, J. Liu, V. C. Leung, and C.-H. Hsu. A survey on cloud gaming: Future of computer games. *IEEE Access*, 4:7605–7620, 2016.
- [7] Q. Cao, S. Zeng, M.-O. Pun, and Y. Chen. Network-level system performance prediction using deep neural networks with cross-layer information. In *Proc. of ICC*, 2020.
- [8] D.-Y. Chen and M. El-Zarki. A framework for adaptive residual streaming for single-player cloud gaming. *ACM TOMM*, 15(2s):1–23, 2019.
- [9] T. Chen, T. Moreau, Z. Jiang, L. Zheng, E. Yan, H. Shen, M. Cowan, L. Wang, Y. Hu, L. Ceze, et al. {TVM}: An automated {End-to-End} optimizing compiler for deep learning. In *OSDI*, pages 578–594, 2018.
- [10] J. Chen et al. Qava: quota aware video adaptation. In *Proc. of ACM CoNext*, 2012.
- [11] S. Choy, B. Wong, G. Simon, and C. Rosenberg. A hybrid edge-cloud architecture for reducing on-demand gaming latency. *Multimedia systems*, 20:503–519, 2014.
- [12] Cirp. <https://cirppapple.substack.com/p/iphone-14-pro-and-pro-max-soar>.
- [13] The worldwide cloud gaming industry is expected to reach \$14 billion by 2027. <https://www.globenewswire.com/news-release/2022/02/10/2382631/28124/en/The-Worldwide-Cloud-Gaming-Industry-is-Expected-to-Reach-14-Billion-by-2027.html#:~:text=The%20Global%20Cloud%20Gaming%20Market,is%20based%20on%20cloud%20technology>.
- [14] Corridor. <https://assetstore.unity.com/packages/essentials/tutorial-projects/corridor-lighting-example-33630#description/>.
- [15] L. Dai, X. Liu, C. Li, and J. Chen. Awnet: Attentive wavelet network for image isp. In *European Conference on Computer Vision*, pages 185–201. Springer, 2020.
- [16] A. Di Domenico, G. Perna, M. Trevisan, L. Vassio, and D. Giordano. A network analysis on cloud gaming: Stadia, geforce now and psnow. *Network*, 1(3):247–260, 2021.
- [17] D. Finkel, M. Claypool, S. Jaffe, T. Nguyen, and B. Stephen. Assignment of games to servers in the onlive cloud game system. In *Proc. of NetGames*, 2014.
- [18] J.-Y. Franceschi, E. Delasalles, M. Chen, S. Lamprier, and P. Gallinari. Stochastic latent residual video prediction. *arXiv preprint arXiv:2002.09219*, 2020.
- [19] H. Fu, H. Yuan, M. Li, Z. Sun, and F. Li. Models and analysis of video streaming end-to-end distortion over lte network. In *2016 IEEE 11th Conference on Industrial Electronics and Applications (ICIEA)*, pages 516–521. IEEE, 2016.

- [20] B. Gajera, S. R. Kapil, D. Ziaei, J. Mangalagiri, E. Siegel, and D. Chapman. Ct-scan denoising using a charbonnier loss generative adversarial network. *IEEE Access*, 9:84093–84109, 2021.
- [21] GeForce Now system requirements. <https://www.nvidia.com/en-us/geforce-now/system-reqs/>, 2022.
- [22] Y. Han, D. Guo, W. Cai, X. Wang, and V. Leung. Virtual machine placement optimization in mobile cloud gaming through qoe-oriented resource competition. *IEEE transactions on cloud computing*, 2020.
- [23] H.-J. Hong, D.-Y. Chen, C.-Y. Huang, K.-T. Chen, and C.-H. Hsu. Qoe aware virtual machine placement for cloud games. In *Proc. of NetGames*, Dec. 2013.
- [24] R. Houdaille et al. Shaping http adaptive streams for a better user experience. In *Proc. of ACM MultiSys*, 2012.
- [25] T. Huang, R.-X. Zhang, C. Zhou, and L. Sun. Qarc: Video quality aware rate control for real-time video streaming based on deep reinforcement learning. In *Proc. of ACM Multimedia*, pages 1208–1216, 2018.
- [26] T.-Y. Huang, R. Johari, N. McKeown, M. Trunnell, and M. Watson. A buffer-based approach to rate adaptation: Evidence from a large video streaming service. *ACM SIGCOMM Computer Communication Review*, 44(4):187–198, 2015.
- [27] J. Jiang, V. Sekar, H. Milner, D. Shepherd, I. Stoica, and H. Zhang. Cfa: A practical prediction system for video qoe optimization. In *NSDI*, pages 137–150, 2016.
- [28] J. Jiang, V. Sekar, and H. Zhang. Improving fairness, efficiency, and stability in http-based adaptive video streaming with festive. In *Proc. of ACM CoNEXT*, 2012.
- [29] J. Kang, S. W. Oh, and S. J. Kim. Error compensation framework for flow-guided video inpainting. In *European Conference on Computer Vision*, pages 375–390. Springer, 2022.
- [30] J. Kaur and S. Das. Future frame prediction of a video sequence. *ArXiv*, abs/2009.01689, 2020.
- [31] J. Kim, Y. Jung, H. Yeo, J. Ye, and D. Han. Neural-enhanced live streaming: Improving live video ingest via online learning. In *Proceedings of the Annual conference of the ACM Special Interest Group on Data Communication on the applications, technologies, architectures, and protocols for computer communication*, pages 107–125, 2020.
- [32] L. Kong, B. Jiang, D. Luo, W. Chu, X. Huang, Y. Tai, C. Wang, and J. Yang. Ifrnet: Intermediate feature refine network for efficient frame interpolation. In *Proc. of CVPR*, pages 1969–1978, 2022.
- [33] W.-S. Lai, J.-B. Huang, N. Ahuja, and M.-H. Yang. Fast and accurate image super-resolution with deep laplacian pyramid networks. *IEEE Transactions on Pattern Analysis and Machine Intelligence*, 41:2599–2613, 2019.
- [34] Z. Lai, Y. C. Hu, Y. Cui, L. Sun, and N. Dai. Furion: Engineering high-quality immersive virtual reality on today’s mobile devices. In *Proc. of MobiCom*, 2017.
- [35] I. Lee, S. Kim, S. Sathyanarayana, K. Bin, S. Chong, K. Lee, D. Grunwald, and S. Ha. R-fec: RI-based fec adjustment for better qoe in webRTC. In *Proc. of MM*, 2022.
- [36] J. Lee, S. Lee, J. Lee, S. D. Sathyanarayana, H. Lim, J. Lee, X. Zhu, S. Ramakrishnan, D. Grunwald, and K. Lee. Perceive: deep learning-based cellular uplink prediction using real-time scheduling patterns. In *Proc. of Mobisys*, 2020.
- [37] K. Lee, D. Chu, E. Cuervo, J. Kopf, Y. Degtyarev, S. Grizan, A. Wolman, and J. Flinn. Outatime: Using speculation to enable low-latency continuous interaction for mobile cloud gaming. In *Proc. of MobiSys*, pages 151–165, 2015.
- [38] Y. Li, X. Tang, and W. Cai. Play request dispatching for efficient virtual machine usage in cloud gaming. *IEEE Trans. Circuits Syst. Video Technol.*, 2015.
- [39] Y. Liao. Learning to predict end-to-end network performance. *PhD thesis*, 2013. <https://hdl.handle.net/2268/136727>.
- [40] M. Marzolla, S. Ferretti, and G. D’angelo. Dynamic resource provisioning for cloud-based gaming infrastructures. *CIE*, 10(1):1–20, 2012.
- [41] R. K. Mok et al. QDASH: a qoe-aware DASH system. In *Proc. of ACM MultiSys*, 2012.
- [42] A. Narayanan, X. Zhang, R. Zhu, A. Hassan, S. Jin, X. Zhu, X. Zhang, D. Rybkin, Z. Yang, Z. M. Mao, F. Qian, and Z.-L. Zhang. A variegated look at 5g in the wild: Performance, power, and qoe implications. In *Proc. of SIGCOMM*, 2021.
- [43] Nature. <https://assetstore.unity.com/packages/3d/environments/nature-starter-kit-2-52977#description/>.
- [44] S. Oprea, P. Martinez-Gonzalez, A. Garcia-Garcia, J. Castro-Vargas, S. Orts-Escolano, J. Garcia-Rodriguez, and A. Argyros. A review on deep learning techniques for video prediction. *arXiv:2004.05214*, 2020. <https://arxiv.org/pdf/2004.05214.pdf>.

- [45] Z. Qi, J. Yao, C. Zhang, M. Yu, Z. Yang, and H. Guan. Vgris: Virtualized gpu resource isolation and scheduling in cloud gaming. *ACM Trans. ACO*, 2014.
- [46] A. Ranjan and M. J. Black. Optical flow estimation using a spatial pyramid network. In *Proc. of CVPR*, pages 4161–4170, 2017.
- [47] F. A. Reda, G. Liu, K. J. Shih, R. Kirby, J. Barker, D. Tarjan, A. Tao, and B. Catanzaro. Sdc-net: Video prediction using spatially displaced convolution. In *Proc. of ECCV*, 2018.
- [48] A. Sankisa, A. Punjabi, and A. K. Katsaggelos. Video error concealment using deep neural networks. In *2018 25th IEEE ICIP*, pages 380–384. IEEE, 2018.
- [49] A. Sankisa, A. Punjabi, and A. K. Katsaggelos. Temporal capsule networks for video motion estimation and error concealment. *Signal, Image and Video Processing*, 14(7):1369–1377, 2020.
- [50] M. Semsarzadeh, M. Hemmati, A. Javadtalab, A. Yassine, and S. Shirmohammadi. A video encoding speed-up architecture for cloud gaming. In *Proc. of IEEE Int. Conf. Multimedia Expo Workshops*, 2014.
- [51] W. Shi, J. Caballero, F. Huszár, J. Totz, A. P. Aitken, R. Bishop, D. Rueckert, and Z. Wang. Real-time single image and video super-resolution using an efficient sub-pixel convolutional neural network. In *Proc. of CVPR*, pages 1874–1883, 2016.
- [52] Y. Sun et al. Cs2p: Improving video bitrate selection and adaptation with data-driven throughput prediction. In *Proc. of ACM SIGCOMM*, 2016.
- [53] Z. Tan, Y. Li, Q. Li, Z. Zhang, Z. Li, and S. Lu. Supporting mobile vr in lte networks: How close are we? In *Proc. MACS*, 2018.
- [54] A. Terwilliger, G. Brazil, and X. Liu. Recurrent flow-guided semantic forecasting. In *Proc. of WACV*, 2019.
- [55] G. Tian and Y. Liu. Towards agile and smooth video adaptation in dynamic HTTP streaming. In *Proc. of CoNEXT*, pages 109–120. ACM, 2012.
- [56] S. Tulyakov, M.-Y. Liu, X. Yang, and J. Kautz. Mocogan: Decomposing motion and content for video generation. In *Proc. of CVPR*, 2018.
- [57] Unity. <https://unity.com/>.
- [58] Rendering pipelin introduction. <https://docs.unity3d.com/Manual/render-pipelines-overview.html>.
- [59] Viking Village. <https://assetstore.unity.com/packages/essentials/tutorial-projects/viking-village-urp-29140#description/>.
- [60] C. Vondrick, H. Pirsiavash, and A. Torralba. Generating videos with scene dynamics. In *Proc. of NeurIPS*, 2016.
- [61] S. Wang, Y. Liu, and S. Dey. Wireless network aware cloud scheduler for scalable cloud mobile gaming. In *Proc. of ICC*, 2012.
- [62] Y. Wang, L. Jiang, M.-H. Yang, L.-J. Li, M. Longand, and L. Fei-Fei. “eidetic 3d lstm: A model for video prediction and beyond. In *Proc. of ICLR*, 2019.
- [63] Y. Wang, H. Wu, J. Zhang, Z. Gao, J. Wang, P. S. Yu, and M. Long. PredRNN: A recurrent neural network for spatiotemporal predictive learning, 2021.
- [64] J. Wu, C. Yuen, N.-M. Cheung, J. Chen, and C. W. Chen. Enabling adaptive high-frame-rate video streaming in mobile cloud gaming applications. *IEEE Trans. on Circuits and Systems for Video Technology*, 25(12):1988–2001, 2015.
- [65] J. Wu, C. Yuen, N.-M. Cheung, J. Chen, and C. W. Chen. Streaming mobile cloud gaming video over tcp with adaptive source–fec coding. *IEEE Transactions on Circuits and Systems for Video Technology*, 27(1):32–48, 2016.
- [66] D. Xu, A. Zhou, X. Zhang, G. Wang, X. Liu, C. An, Y. Shi, L. Liu, and H. Ma. Understanding operational 5g: A first measurement study on its coverage, performance and energy consumption. In *Proceedings of the Annual conference of the ACM Special Interest Group on Data Communication on the applications, technologies, architectures, and protocols for computer communication*, pages 479–494, 2020.
- [67] H. Yeo, C. J. Chong, Y. Jung, J. Ye, and D. Han. Nemo: enabling neural-enhanced video streaming on commodity mobile devices. In *Proceedings of the 26th Annual International Conference on Mobile Computing and Networking*, pages 1–14, 2020.
- [68] H. Yeo, Y. Jung, J. Kim, J. Shin, and D. Han. Neural adaptive content-aware internet video delivery. In *13th {USENIX} Symposium on Operating Systems Design and Implementation ({OSDI} 18)*, pages 645–661, 2018.
- [69] H. Yeo, H. Lim, J. Kim, Y. Jung, J. Ye, and D. Han. Neuroscaler: neural video enhancement at scale. In *Proceedings of the ACM SIGCOMM 2022 Conference*, pages 795–811, 2022.

- [70] X. Yin, A. Jindal, V. Sekar, and B. Sinopoli. A control-theoretic approach for dynamic adaptive video streaming over http. In *SIGCOMM*. ACM, 2015.
- [71] C. Yu, Y. Xu, B. Liu, and Y. Liu. “can you see me now?” a measurement study of mobile video calls. In *IEEE INFOCOM 2014-IEEE Conference on Computer Communications*, pages 1456–1464. IEEE, 2014.
- [72] W. Yu, Y. Lu, S. Easterbrook, and S. Fidler. Efficient and information-preserving future frame prediction and beyond. In *ICLR*, 2020.
- [73] W. Yu, Y. Lu, S. M. Easterbrook, and S. Fidler. Crevnet: Conditionally reversible video prediction. *ArXiv*, abs/1910.11577, 2019.
- [74] C. Zhang, Z. Qi, J. Yao, M. Yu, and H. Guan. vgas: Adaptive scheduling algorithm of virtualized gpu resource in cloud gaming. *IEEE Trans. on Parallel Distrib. Syst.*, 2014.
- [75] J. Zhang, Y. Wang, M. Long, W. Jianmin, and P. S. Yu. Z-order recurrent neural networks for video prediction. In *Proc. of ICME*, 2019.